Supplementary Methods

TEVC charge-substrate ratio measurements. [^{3}H]Arg was mixed with unlabeled Arg and applied to PQLC2 oocytes at 3 mM concentration and 5-15 dpm/pmol specific activity as a trade-off between current and Arg accumulation measurements. PQLC2 and mock oocytes clamped at -40 mV were perfused at pH 5.0 with [^{3}H]Arg for varying durations, and washed with ND100 buffered with 5 mM HEPES at pH 7.5 instead of pH 5.0 to inactivate PQLC2 and prevent loss of internal [^{3}H]Arg by PQLC2 reversal during the washing step. Oocytes were then disimpaled, washed 4 times with ice-cold ND100 pH 7.5 and lysed in 0.1 N NaOH. Intracellular radioactivity was counted using a Tri-Carb 2100 TR liquid scintillation analyzer (Packard). To measure the accumulated charge, the Arg-evoked current was integrated over time from the start of [^{3}H]Arg application to the end of the wash step.

Reversal potential measurements. PQLC2 oocytes were hold at -20 mV with a repetition of the voltage jump protocol (see main text) every 20 s. Lys or Arg (20 mM) was applied at pH 5.00 for 5 to 15 min to build up $[CAA]_{in}$. After a brief wash, varied CAA_{out} concentrations were applied: 0.2; 0.7; 2; 7 and 20 mM for Lys, and 0.5; 1; 2; 5; 10 and 20 mM for Arg. The contribution of CAA leaking from the oocyte (grey dashed line in Fig. 2C,D) was well below these concentration ranges. The last 20 mM application was used to verify that $[CAA]_{in}$ remained stable throughout the measurements. The stability of successive I-V curves in a given medium was used to verify that $[CAA]_{out}$ had fully equilibrated around the oocyte.

Ion-selective electrode measurements. Recordings were made under TEVC as above with a third intracellular ion-selective electrode connected to a high gain, low noise, custom-made electrometer (42). To prepare the intracellular pH electrode, a silanized micropipette was tip-filled with a proton ionophore (Hydrogen ionophore I, cocktail B, Sigma-Aldrich) and backfilled with: 150 mM NaCl; 40 mM KH_2PO_4; 23 mM NaOH, pH 6.8. The positive and negative inputs of the electrometer were connected to the pH electrode and the voltage ground electrode of the TEVC setup, respectively. The potential difference between the two inputs tested in diverse buffers (pH range: 5.0-7.0) was proportional to pH with a mean slope of -72 ± 5 mV (n = 4). The variable amplitude of the His-evoked response in PQLC2 oocytes (Fig. S1E,F) and the variable speed of potential return to baseline upon His washout (compare Fig. 1B and S1D) may reflect different PQLC2 densities in the oocyte membrane and different impalement depths of the pH electrode.

BCECF-based pH_{in} recording. Oocytes were injected with 45 ng of PQLC2-LL290/291AA-EGFP cRNA or their nucleus was injected with 2.5 ng cDNA in a 5-nl volume using a custom-made injector. After 2-3 days incubation at 17 °C, oocytes were selected under a fluorescence microscope. Only oocytes with strong green membrane fluorescence at the animal pole were injected with 25 nl saturated aqueous BCECF (Invitrogen, UK). The injected BCECF dominated the EGFP fluorescence thereafter. Proton transport was measured in 100 mM Na-gluconate, 4 mM $MgSO_4$, 2 mM K-gluconate buffered at pH 7.5 (HEPES-NaOH) or pH 6.0 (MES-NaOH) by simultaneous TEVC using a TEC10C (npi, Tamm, Germany) amplifier and fluorescence acquisition with a "Fluorocyte device" as described (43), except that the mostly pigment-free

equator of the yellow pole was facing downward towards the fluorescence pathway, and the photodiode amplifier had a transimpedance gain of 1 GV/A. Oocytes were either clamped at -100 mV or stepped from 0 (100 ms) to +20 or -120 mV (400 ms). Solutions were switched using a custom-built valve bank and the setup was controlled via a National Instruments USB-6221 interface, with WinWCP version 4.5.0 (developed by Dr. John Dempster, University of Strathclyde, UK). Substrate currents were induced by different concentrations of pH-adjusted arginine, lysine, histidine or canavanine, as indicated. Data were analyzed using WinWCP, filtered in pClamp 9.0 and plotted with Origin 7.0 or Excel.

Whole-cell patch-clamp recording in HEK293T cells. HEK293T cells grown in DMEM supplemented with GlutaMAX, 10% Fetal Bovine Serum and 100 units/mL Penicillin-Streptomycin (GIBCO) were transfected using lipofectamine 2000 (Thermofisher) with a modified pEGFP-N1 plasmid (Clontech) encoding PQLC2-LL290/291AA-EGFP (14). 24h after transfection, cells were transferred in 35-mm culture dishes (Falcon, Fisher Scientific) coated with poly-D-Lysine (Sigma-Aldrich) at 150 000 cells per dish. Whole-cell patch-clamp recording were done at least 4h after the transfer at room temperature using an EPC-9 amplifier controlled via Patchmaster software (HEKA Elektronik, Germany) and a fast perfusion system, as described (44). Recordings were sampled at 5 kHz and not filtered. Isolated HEK293T cells expressing PQLC2-LL290/291AA-EGFP were identified under LED illumination. Only cells with an input resistance over 300 MΩ were analyzed. Cells were clamped at -40 mV. I-V curves were determined using a voltage ramp protocol (30 ms at -100 mV, followed by a 400-ms ramp from -100 mV to +100 mV) applied before, during and after each CAA application. Non-fluorescent cells from the same dish were used as negative controls.

Amino acid measurements by liquid chromatography coupled to high-resolution mass spectrometry (LC–HRMS). Oocytes perfused or not for 5 min with 20 mM Lys at -60 mV and pH 5.0 were washed 4 times with ice-cold ND100 pH 7.5, flash frozen in liquid nitrogen and kept at -20 °C. To analyze their contents, oocytes were lysed by repeated pipetting in 100 µL cold methanol:water (1:1) and centrifuged for 5 min at 16,000 *g* at 4 °C. 80 µL of supernatant was dessicated in a Vacufuge Plus (Eppendorf) and kept at -20°C. Before analysis by LC-HRMS, dried extracts were reconstituted in 40 µL of water containing 0.1% formic acid. Amino acid analyses were conducted essentially as described (45), using a Dionex Ultimate chromatographic system (Thermo Fisher Scientific, Courtaboeuf, France) coupled to an Exactive (Orbitrap) high resolution mass spectrometer from Thermo Fisher Scientific (Courtaboeuf, France) fitted with an electrospray ion source. Chromatographic separation was performed on a Discovery HS F5 PFPP 5 µm, 2.1 × 250 mm column (Sigma, Saint Quentin Fallavier, France) at 30°C and using a flow rate of 250 µL/min. The chromatographic system was equipped with an on-line prefilter (Thermo Fisher Scientifics, Courtaboeuf, France). Mobile phases A and B were water with 0.1% formic acid and acetonitrile with 0.1% formic acid, respectively. After sample injection (15 µL), elution started with an isocratic step of 2 min at 5% phase B, followed by a linear gradient from 5 to 100% of phase B in 18 min. These proportions were kept constant for 4 min before returning to 5% of phase B and letting the system equilibrate for 6 min. The column effluent was directly introduced into the electrospray source of the mass spectrometer operated in the positive ion mode. Source parameters were as follows: capillary voltage set at 5 kV, capillary temperature at 300 ◦C; sheath and auxiliary gas (nitrogen) flow rates at 50 and 25 arbitrary units, respectively; mass resolution power of the analyzer set at 50,000 at *m/z* 200 (full width at half maximum, FWHM). The

acquisition was achieved from *m/z* 50 to 250. Extracted ion chromatograms were generated for each amino acid resulting peaks integrated using the Xcalibur software (version 2.1, Thermo Fisher Scientific).

Kinetic modeling, rate constant equations. Voltage dependence was implemented in the rate constants of the uniporter model using the following equations, where β_o, γ_o, δ, ε, γ_i and β_i represent the dielectric displacement of the charged substrate (S^+) in the voltage gradient during its translocation across the membrane, and η and θ represent the charge displacement in the protein during rearrangement of the outer and inner gates, respectively (Fig. S4A):

- *Charged substrate (S^+) local concentration near the binding site (Woodhull effect):*

$$[S^+]_{o.loc} = [S^+]_{o.bulk} \cdot e^{-\frac{\beta_o.F \cdot V}{RT}}$$
$$[S^+]_{i.loc} = [S^+]_{i.bulk} \cdot e^{-\frac{\beta_i.F \cdot V}{RT}}$$

- *Substrate binding:*

$$k_{o.on} = k_{o.on(0)} \cdot [S^+]_{o.loc} \cdot e^{-\frac{\gamma_o.F \cdot V}{2RT}}$$
$$k_{o.off} = k_{o.off(0)} \cdot e^{\frac{\gamma_o.F \cdot V}{2RT}}$$
$$K_{D.out} = k_{o.off}/k_{o.on}$$
$$k_{i.on} = k_{i.on(0)} \cdot [S^+]_{i.loc} \cdot e^{\frac{\gamma_i.F \cdot V}{2RT}}$$
$$k_{i.off} = k_{i.off(0)} \cdot e^{-\frac{\gamma_i.F \cdot V}{2RT}}$$
$$K_{D.in} = k_{i.off}/k_{i.on}$$

- *Structural transitions in apo state:*

$$k_{o.op} = k_{o.op(0)} \cdot e^{\frac{\eta.F \cdot V}{2RT}}$$
$$k_{o.cl} = k_{o.cl(0)} \cdot e^{-\frac{\eta.F \cdot V}{2RT}}$$
$$k_{i.op} = k_{i.op(0)} \cdot e^{-\frac{\theta.F \cdot V}{2RT}}$$
$$k_{i.cl} = k_{i.cl(0)} \cdot e^{\frac{\theta.F \cdot V}{2RT}}$$

- *Structural transitions in loaded state:*

$$k^S_{o.op} = k^S_{o.op(0)} \cdot e^{\frac{(\eta+\delta\cdot\epsilon).F \cdot V}{2RT}}$$
$$k^S_{o.cl} = k^S_{o.cl(0)} \cdot e^{-\frac{(\eta+\delta\cdot\epsilon).F \cdot V}{2RT}}$$
$$k^S_{i.op} = k^S_{i.op(0)} \cdot e^{-\frac{(\theta+\delta\cdot(1-\epsilon)).F \cdot V}{2RT}}$$
$$k^S_{i.cl} = k^S_{i.cl(0)} \cdot e^{\frac{(\theta+\delta\cdot(1-\epsilon)).F \cdot V}{2RT}}$$

In the simulations shown in Fig. 7C, cytosolic gate equations were modified as follows to implement an asymmetrical energy barrier:

$$k_{i.op} = k_{i.op(0)} \cdot e^{-0.2\times\frac{\theta.F\cdot V}{RT}}$$

$$k_{i.cl} = k_{i.cl(0)} \cdot e^{0.8\times\frac{\theta.F\cdot V}{2RT}}$$

$$k^{S}_{i.op} = k^{S}_{i.op(0)} \cdot e^{-\frac{(0.2\times\theta+0.5\times\delta\cdot(1-\epsilon)).F\cdot V}{RT}}$$

$$k^{S}_{i.cl} = k^{S}_{i.cl(0)} \cdot e^{\frac{(0.8\times\theta+0.5\times\delta\cdot(1-\epsilon)).F\cdot V}{RT}}$$

Supplementary references

42. Picollo A, Pusch M (2005) Chloride/proton antiporter activity of mammalian CLC proteins ClC-4 and ClC-5. *Nature* 436(7049):420–423.

43. Zdebik AA, et al. (2008) Determinants of anion-proton coupling in mammalian endosomal CLC proteins. *J Biol Chem* 283(7):4219–4227.

44. Blarre T, Bertrand HO, Acher FC, Kehoe JS (2014) Molecular determinants of agonist selectivity in glutamate-gated chloride channels which likely explain the agonist selectivity of the vertebrate glycine and GABAa-ρ receptors. *PLoS One* 9(12):e115788.

45. Rubio-Patiño C, et al. (2018) Low-Protein Diet Induces IRE1α-Dependent Anticancer Immunosurveillance. *Cell Metab* 27(4):828-842.e7.

Supplementary Figure Legends

Fig S1: Fluorometric and ion-selective electrode pH_{in} recording of PQLC2. (A-C) PQLC2 oocytes were injected with the pH probe BCECF and recorded for fluorescence under voltage clamp at pH 6.0. (A) Representative current and BCECF fluorescence traces of a PQLC2 perfused by 5 mM Arg and 10 mM His. The oocyte was hyperpolarized during amino acid perfusion to accelerate PQLC2 and confirm the acidification response induced by His (green arrows). (B) Mean BCECF responses to Arg and His. *, $P < 0.05$; ** P, 0.01 (C) Representative current and BCECF fluorescence traces of a PQLC2 perfused by 5 mM Arg and 10 mM canavanine (Can). Canavanine induces an acidification (purple arrows), in agreement with its side-chain pK_a. (D-F) Additional pH electrode recording data. (D) Current and pH electrode traces of the PQLC2 oocyte shown in Fig. 1C. (E) H^+-selective electrode responses evoked in PQLC2 oocytes perfused at pH 5.0 with either 20 mM His and Arg or 20 mM His and Lys. (F) PQLC2 oocytes were perfused with increasing His concentrations as in D. The graphs show the slope and current threshold of the linear regression of the acidification-current relationship observed for His concentrations ≥ 4 mM (see red dashed line in Fig. 1C).

Fig S2: Arg_{out} inwardly rectifies the PQLC2 current. (A) Raw traces of the currents shown in Fig. 3E. (B) Representative evoked current traces induced by sequential application of 20 mM Lys and Arg to a PQLC2 oocyte. (C) Relationship between the inward current evoked by either Lys or Arg (20 mM) at -80 mV and the outward current measured during the subsequent washing step at +40 mV. Each symbol represents a unique PQLC2 oocyte. (D) Mean I-V curves for successive applications of either Lys or Arg (20 mM) to PQLC2 oocytes. (E) Representative current traces in whole-cell patched-clamp HEK293 cells expressing, or not, PQLC2 at their surface. Cells were filled with either 20 mM NMDG or 20 mM Lys through the patch-clamp micropipette. (F) Average I-V curves recorded in mock cells. (G) Individual I-V curves recorded in two PQLC2 cells filled with either NMDG or Lys.

Fig S3: Substrate concentration dependence of the PQLC2 current. Arg- and Lys-filled PQLC2 oocytes were subjected to voltage jumps at pH 5.0 in the presence of varying concentration of the corresponding substrate. (A, B) Concentration dependence of the inward and outward currents at -80 and +80 mV, respectively. The inward and outward currents of each oocyte were normalized to their values at $[CAA]_{out} = \infty$ and 0 mM, respectively. (C) Eadie-Hofstee plots of the data shown in A,B.

Fig S4: Kinetic modeling of PQLC2. (A) Rate constants and voltage-dependence parameters of the 6-state electrogenic uniporter model. The right scheme shows the energy profile of the charged substrate along the translocation pathway, with the corresponding voltage-dependence parameters. (B) Systematic study of the impact of voltage-dependent parameters on the current-voltage relationship. A set of parameters yielding monotonic I-V curves was selected as a plausible model of PQLC2. (C) I-V curves of the 16

substrates at 20 and 0 mM luminal and cytosolic concentrations, respectively. The curves of S3 and S11 are colored in blue and red, respectively. (D) I-V curves of S3 and S11 in the initial model for the indicated conditions. (E) The reservoir filling data shown in Fig. 6D were replotted to compare the cytosol-facing site occupancy ($K_{D.in}$ = 1 mM for both substrates) with the loading current inhibition. (F) Duplicated cycle used to detect exchange cycles in MarkovEditor.

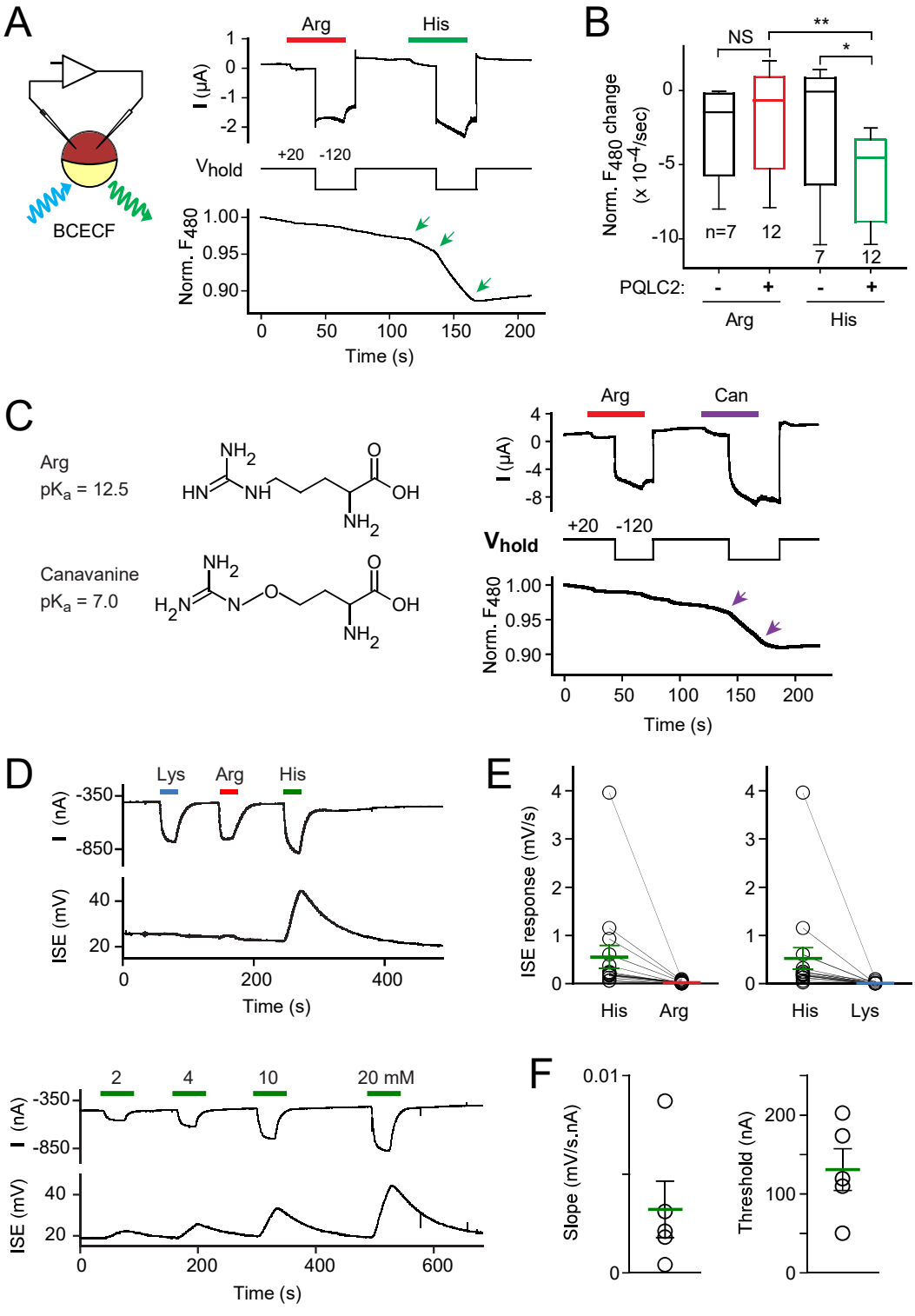
A
BCECF
Arg
His
I (μA)
Vhold
+20
-120
Norm. F480
Time (s)
B
NS
**
*
Norm. F480 change
(x 10-4/sec)
n=7
12
7
12
PQLC2:
Arg
His
C
Arg
pKa = 12.5
Canavanine
pKa = 7.0
Can
D
Lys
Arg
His
I (nA)
ISE (mV)
Time (s)
2
4
10
20 mM
E
ISE response (mV/s)
His
Arg
Lys
F
Slope (mV/s.nA)
Threshold (nA)

Figure S1

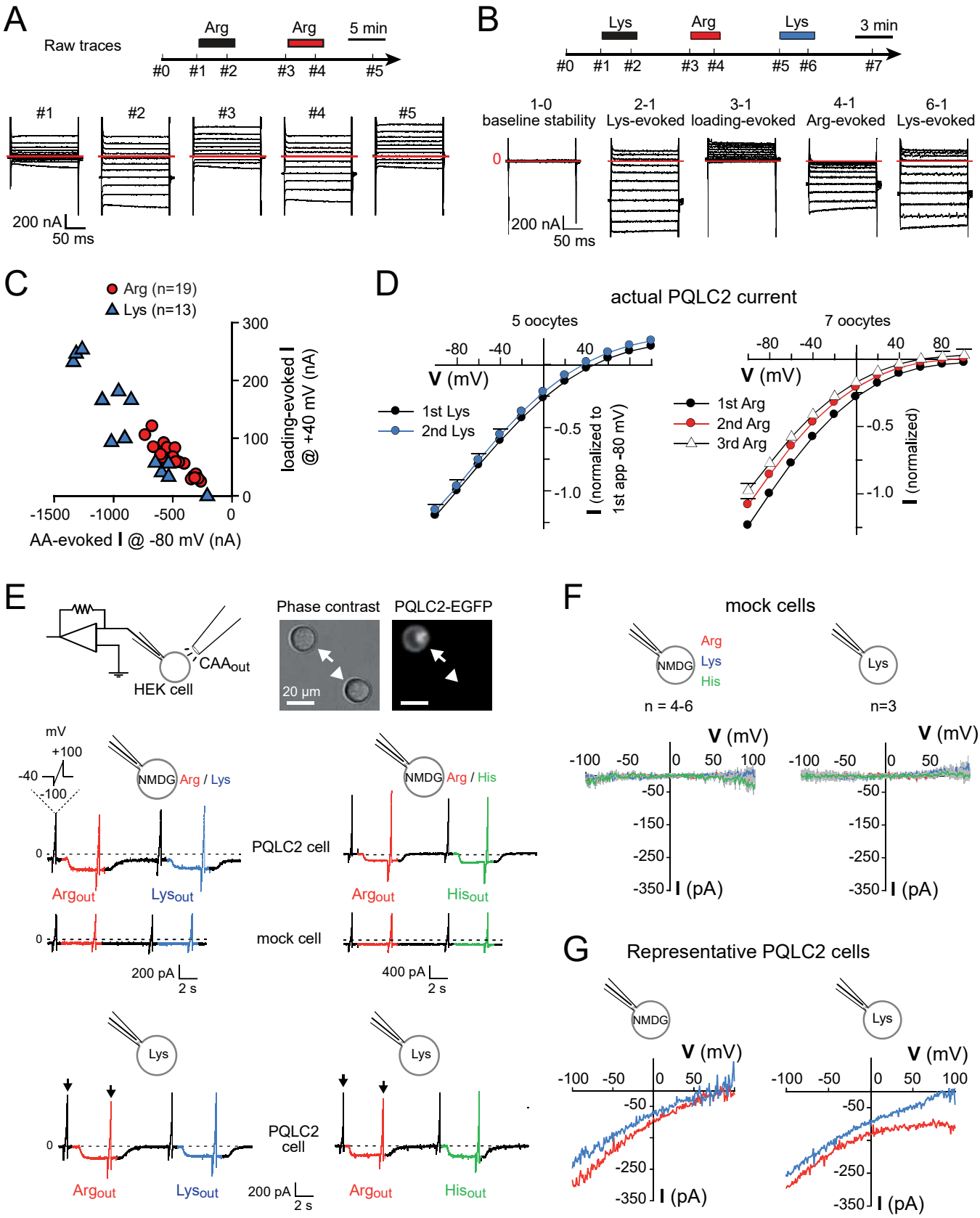
A
Raw traces
Arg
Arg
5 min
#0 #1 #2 #3 #4 #5
#1 #2 #3 #4 #5
200 nA
50 ms
B
Lys
Arg
Lys
3 min
#0 #1 #2 #3 #4 #5 #6 #7
1-0 baseline stability
2-1 Lys-evoked
3-1 loading-evoked
4-1 Arg-evoked
6-1 Lys-evoked
0
200 nA
50 ms
C
Arg (n=19)
Lys (n=13)
loading-evoked I @ +40 mV (nA)
AA-evoked I @ -80 mV (nA)
D
actual PQLC2 current
5 oocytes
7 oocytes
V (mV)
1st Lys
2nd Lys
1st Arg
2nd Arg
3rd Arg
I (normalized to 1st app -80 mV)
I (normalized)
E
HEK cell
CAA_out
Phase contrast
PQLC2-EGFP
20 µm
mV
+100
-40
-100
NMDG Arg / Lys
NMDG Arg / His
PQLC2 cell
mock cell
Arg_out
Lys_out
His_out
200 pA
400 pA
2 s
Lys
PQLC2 cell
F
mock cells
NMDG
Arg
Lys
His
n = 4-6
n=3
V (mV)
I (pA)
G
Representative PQLC2 cells
NMDG
Lys
V (mV)
I (pA)

Figure S2

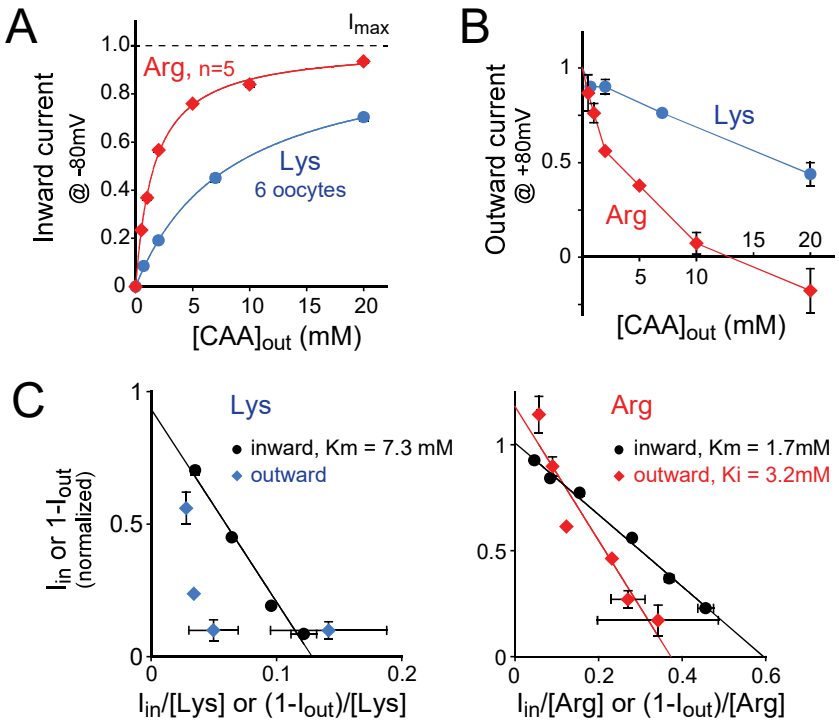
A
Imax
Arg, n=5
Lys
6 oocytes
Inward current
@ -80mV
[CAA]out (mM)
B
Outward current
@ +80mV
Lys
Arg
[CAA]out (mM)
C
Lys
inward, Km = 7.3 mM
outward
Iin or 1-Iout
(normalized)
Iin/[Lys] or (1-Iout)/[Lys]
Arg
inward, Km = 1.7mM
outward, Ki = 3.2mM
Iin/[Arg] or (1-Iout)/[Arg]

Figure S3

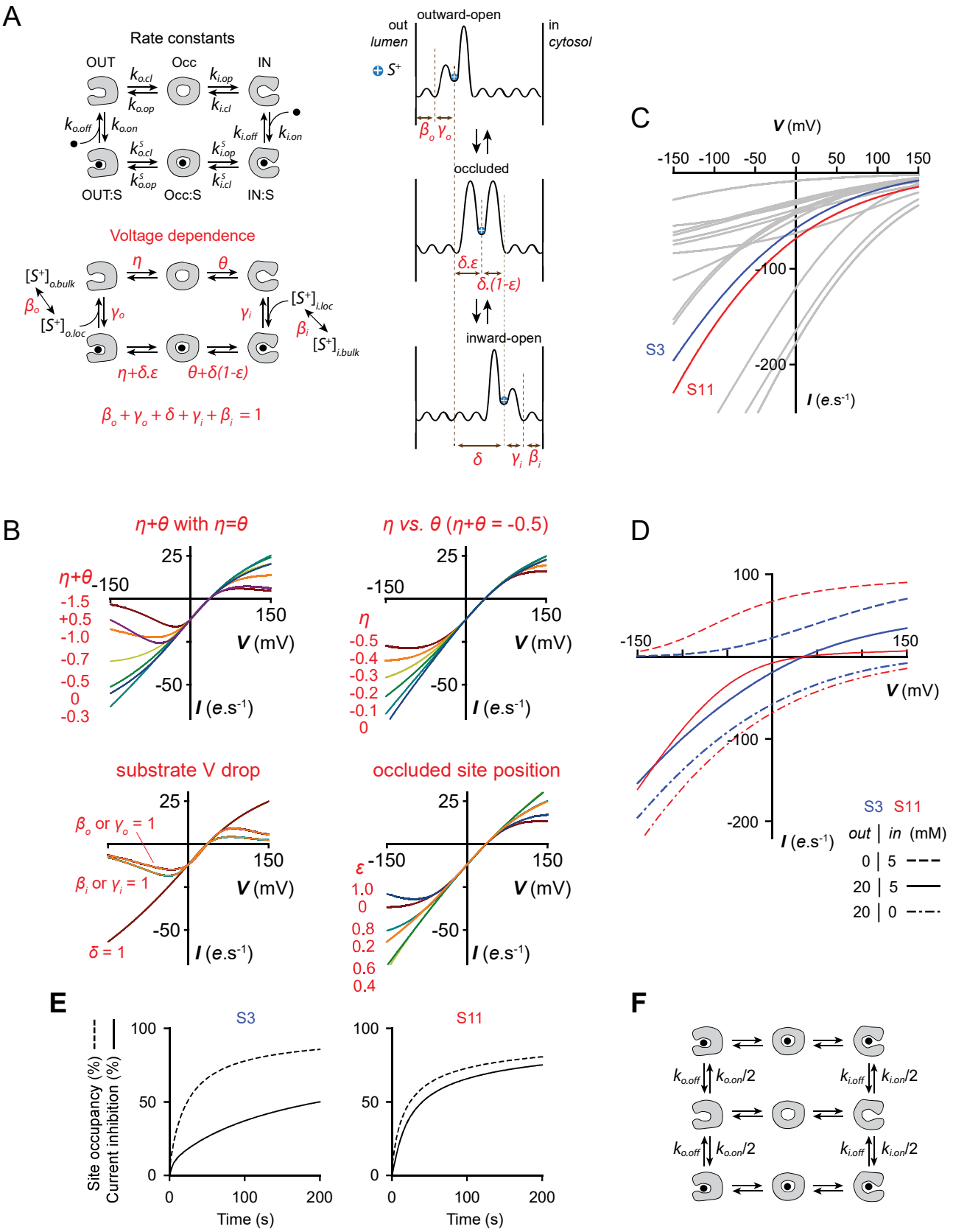
A
Rate constants
OUT
Occ
IN
OUT:S
Occ:S
IN:S
Voltage dependence
$\beta_o + \gamma_o + \delta + \gamma_i + \beta_i = 1$
out
lumen
in
cytosol
outward-open
occluded
inward-open
B
η+θ with η=θ
η vs. θ (η+θ = -0.5)
substrate V drop
occluded site position
V (mV)
I (e.s-1)
C
S3
S11
D
S3 S11
out | in (mM)
0 | 5
20 | 5
20 | 0
E
S3
S11
Site occupancy (%)
Current inhibition (%)
Time (s)
F

Figure S4

Table S1. Uniporter model parameters

Parameter description	Symbol	Unit	Initial model			Refined model	
			General	Substrate # 3	Substrate # 11	Substrate # 3	Substrate # 11
Outer gate charge × dielectric displacement	η	dimensionless	-0.2			-0.1	
Inner gate charge × dielectric displacement	θ	dimensionless	-0.3			-0.4	
Fractional voltage drop along outer access channel	β_o	dimensionless	0			0	
Fractional voltage drop upon binding to outer site	γ_o	dimensionless	0			0	
Dielectric distance between outward- and inward-facing sites	δ	dimensionless	1			1	
Relative position of occluded site	ε	dimensionless	0.2			0.2	
Fractional voltage drop upon binding to inner site	γ_i	dimensionless	0			0	
Fractional voltage drop along inner access channel	β_i	dimensionless	0			0	
Outer substrate association	$k_{o.on}$	$M^{-1}.s^{-1}$	10^9			10^9	
Outer substrate dissociation	$k_{o.off}$	s^{-1}	10^4 to 10^8	10^7	10^6	10^7	10^6
Inner substrate association	$k_{i.on}$	$M^{-1}.s^{-1}$	10^9			10^9	
Inner substrate dissociation	$k_{i.off}$	s^{-1}	10^6			10^6	
Outer gate opening, apo	$k_{o.op}$	s^{-1}	10^3			10^3	
Outer gate closing, apo	$k_{o.cl}$	s^{-1}	10^3			10^3	
Inner gate opening, apo	$k_{i.op}$	s^{-1}	3×10^3			3×10^3	
Inner gate closing, apo	$k_{i.cl}$	s^{-1}	3×10^3			3×10^3	
Outer gate opening, loaded	$k_{o.op}^S$	s^{-1}	100 or 10^3	100	100	50	50
Outer gate closing, loaded	$k_{o.cl}^S$	s^{-1}	100 or 10^3	10^3	10^3	10^3	10^3
Inner gate opening, loaded	$k_{i.op}^S$	s^{-1}	100 or 10^3	100	100	100	100
Inner gate closing, loaded	$k_{i.cl}^S$	s^{-1}	100 or 10^3	100	10^3	200	2×10^3

For each model, parameters are listed in the first column. Other columns only show the values changed for specific substrates.